ACS OMEGA

http://pubs.acs.org/journal/acsodf

Article

Biocompatible pH-Degradable Functional Capsules Based on Melamine Cyanurate Self-Assembly

Nfayem Imoro, Vladimir V. Shilovskikh, Pavel V. Nesterov, Alexandra A. Timralieva, Dmitry Gets, Anna Nebalueva, Filipp V. Lavrentev, Alexander S. Novikov, Nikolay D. Kondratyuk, Nikita D. Orekhov, and Ekaterina V. Skorb*

Cite This: *ACS Omega* 2021, 6, 17267−17275

Read Online

ACCESS | Metrics & More | Article Recommendations | Supporting Information

ABSTRACT: Development of adaptive self-regulating materials and chemical−biological systems—self-healing, self-regulating, etc.—is an advanced modern trend. The very sensitive pH-controlled functionality of supramolecular assemblies is a very useful tool for chemical and biochemical implementations. However, the assembly process can be tuned by various factors that can be used for both better functionality control and further functionalization such as active species, e.g., drugs and dyes, and encapsulation. Here, the effect of a dye, sodium fluorescein (uranine) (FL), on the formation of a self-assembled melamine cyanurate (M−CA) structure is investigated and calculated with density functional theory (DFT) and molecular dynamics. Interestingly, the dye greatly affects the self-assembly process at early stages from the formation of dimers, trimers, and tetramer to nucleation control. The supramolecular structure disassembly and subsequent release of trapped dye occurred under both high- and low-pH conditions. This system can be used for time-prolonged bacterial staining and development of supramolecular capsules for the system chemistry approach.

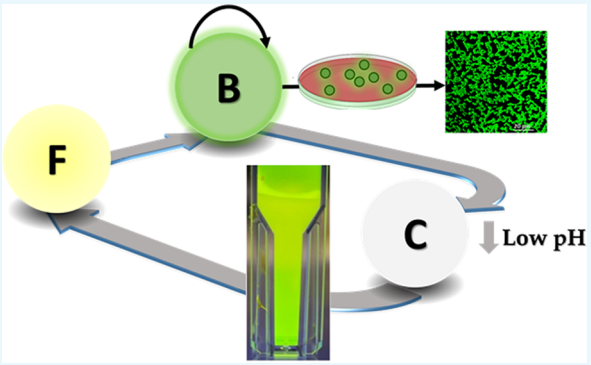

INTRODUCTION

Encapsulating systems are used for drug delivery and tissue engineering applications, wherein they serve as sensors, membranes, and attractive self-healing and antifouling materials.[1] They also protect active chemicals, cells, and biomolecules from interacting with an aggressive environment or regulate their activity via internal or external stimuli.[2,3] The cooperativity principle between living bacteria and materials is key priority.[4] The study presents the bacteria-controlled release of an encapsulated dye (sodium fluorescein (uranine) (FL)) from supramolecular melamine cyanurate (M−CA) structures.

Self-assembly based on nonlinear kinetics is a common feature of living organisms easily depicted by morphogenesis. Controlling this mechanism is one of the key challenges in developing synthetic metabolic networks.[5] Supramolecular structures, e.g., M−CA, are interesting for stimuli-responsive trapping or encapsulation of active species. Formation of M−CA has been observed to be unfavored in too acidic or too basic media. It was recently shown that the initial ratio of reagents influences crystallinity of M−CA self-assembly; however, no evidence of the formation of any other product than stoichiometric 1:1 adduct was shown.[6] Instead, it is more likely to occur in a medium with a favorable pH range between pH 5.0 and 7.5[7] mainly due to both melamine and cyanuric acid existing in their free forms in this range.[8] Therefore, moderate changes in the pH will favor ionic forms of the organic molecules that can influence both the diffusion coefficient and the rate of aggregation (by frustrating the formation of hydrogen-bonded aggregates).

Capsules based on supramolecular self-assembly can be functionalized or modified to include chemical groups that provide ancillary functions[9] or simply sequester and concentrate other organic compounds of interest via intermolecular interactions. A pH-sensitive dye can be used to study the kinetics of these supramolecular capsules. FL and its derivatives, in the dianion form, have a pK_a of ca. 6.68[10] and a pH-dependent analytical wavelength range from 437 to 490 nm[11,12] which makes it a good dye to study the effect of pH on the assembly of M−CA capsules. In addition, successful demonstration of the release of encapsulated fluorescent dye molecules in M−CA capsules due to localized acidification induced by adhering bacteria[13] sets the premise for this

Received: March 2, 2021
Accepted: June 8, 2021
Published: June 25, 2021

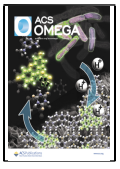

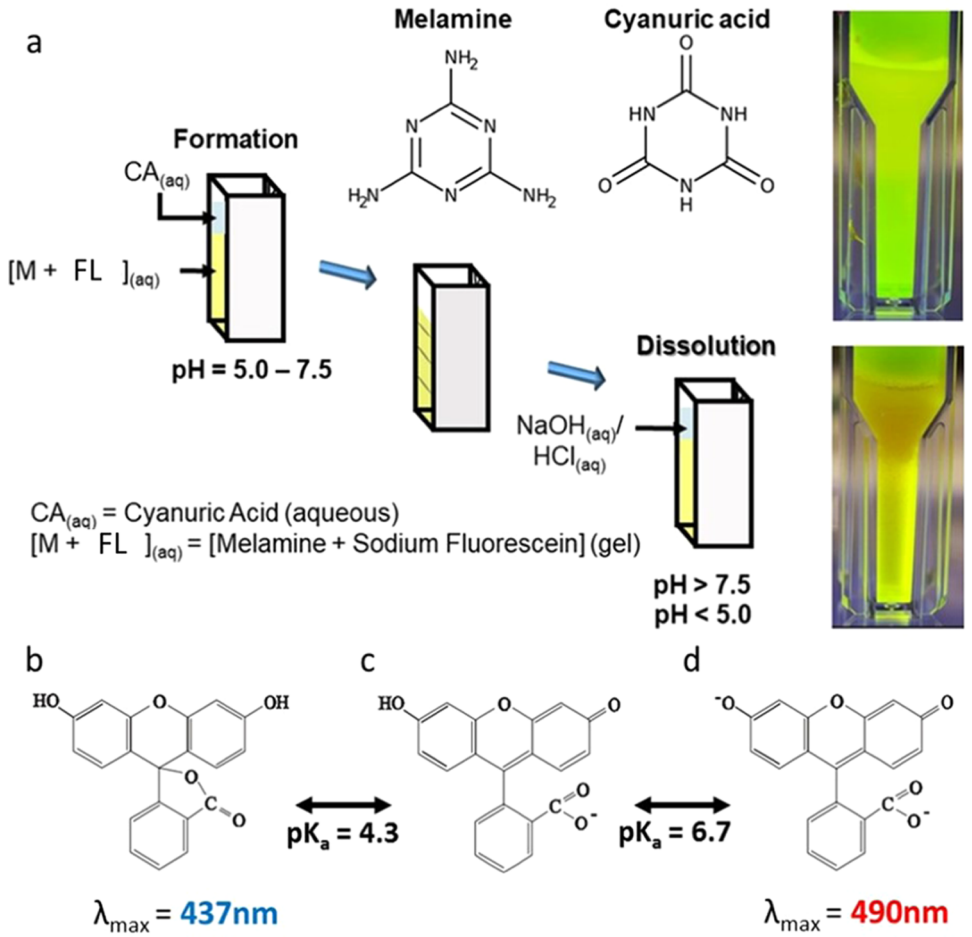

Figure 1. (a) Schematic illustrating the experiment of the reaction-diffusion system of melamine (M) (1 mM in gel) and cyanuric acid (CA) (10 mM in aqueous phase) assembly in the presence of sodium fluorescein (FL) (10^{-4} M in gel) presented on the left and optical photos of plastic cuvettes used for photometric study without (top) and with the assembled structure (bottom) presented on the right. Underneath are prototropic forms of fluorescein responsible for photophysical properties observed in experiments, namely, (b) lactone, (c) monoanion, and (d) dianion.

encapsulation system to be used for analytical studies and future applications in controlled release of sequestered or encapsulated chemical compounds of interest like biocides.

M−CA is often reported as a flame retardant.[14,15] When used as a two-dimensional (2D) molecular sheet, the hexagonal M−CA array is highly effective at providing protection from oxidation for black phosphorus, an optoelectronic material, under ambient conditions over a period of more than a month.[15,16] The rosette structure of melamine cyanurate has also been investigated for its use as a molecular channel or extended columnar structure.[17] The use of M−CA as a capsule for sustained and controlled release of the target substance is hardly documented. However, calix[4]arene dimelamine derivative has been reacted with diethylbarbiturate molecules to produce a molecular receptor for selective encapsulation of different anthraquinone derivatives through self-assembly.[17] This study analyzed both pH and spectral characteristics of the reaction-diffusion self-assembly and disassembly of melamine cyanurate using UV−vis spectrophotometry. Afterward, the prospect of a self-regulated system of bacteria culture and capsule disassembly for bacteria staining was assessed.

RESULTS AND DISCUSSION

Generally, an experimental setup containing M−CA and fluorescein isothiocyanate (FITC) appears as heavily colored clusters in transparent agarose media. Due to densely colored clusters, FL is suspected to be incorporated as a building material in their formation (Figure 1a). A possible explanation is that dye molecules are locked within the M−CA structure and stabilized by a web of characteristic noncovalent bonds.[18] The reaction between M and CA took place in a specially designed setup, which allows observation of diffusion-controlled formation of melamine cyanurate. A typical experiment was conducted with 1 mM melamine embedded in 1% w/v agarose gel with or without FL at a concentration between 10^{-6} and 10^{-4} M inclusive (Figure S1). CA at a concentration of 10 mM is then diffused through the hydrogel to form M−CA capsules. In contrast to fluorescent agarose gel containing M, M−CA capsules did not form upon addition of 10 mM CA to a fluorescent agarose gel without M.

As stated previously FL and its derivatives have photophysical properties such as absorption spectra that can vary as a result of the change in pH (Figure 1b−d), hydrogen bonding strength, and polarity of the environment.[19] This as well as chemical properties that increase its binding affinity to functional biomolecules makes it a good fluorophore to study the pH effect on organic supramolecular structures like

https://doi.org/10.1021/acsomega.1c01124
ACS Omega 2021, 6, 17267−17275

M−CA. The pK_a values of 4.3 and 6.7 represent lactone/monoanion and monoanion/dianion transitions, respectively. These transitions were more likely to occur due to the range of pH determined during assembly and disassembly of capsules (Figure S2). Monoanion and dianion forms have been determined to be the only absorbing species present at pH 5.5−6.4[11] with the strongest absorptivity associated with the dianion at an analytical wavelength of 490 nm.[10] Lactone is formed from lactonization of the cation form, and this lowers the absorbance of the cation that has the strongest absorptivity at an analytical wavelength of 437 nm.[11] To confirm the ability of FL to beneficially bind to M−CA, a series of modeling experiments were performed. In addition, it was shown that M−CA self-assembly in the presence of FL does not lose the ability to form its characteristic structure.

Density Functional Theory (DFT) Analysis of Melamine Cyanurate Capsule Containing Fluorescent Dye Molecules. The quantum chemical computation method was utilized for modeling various adducts of FL, melamine (M), and cyanuric acid (CA) (see Experimental Section for details). Full geometry optimization and Gibbs free energy calculations were carried out for all possible dimer, trimer, tetramer, and rosette-shaped forms of M and CA complexes as well as for dimer, trimers, and individual M and CA associations with FL. The Gibbs free energies of associations were calculated considering that complexes were forming from the most probable predecessors and all interactions are bimolecular. The self-assembly process of M−CA (Figure 2), on the contrary,

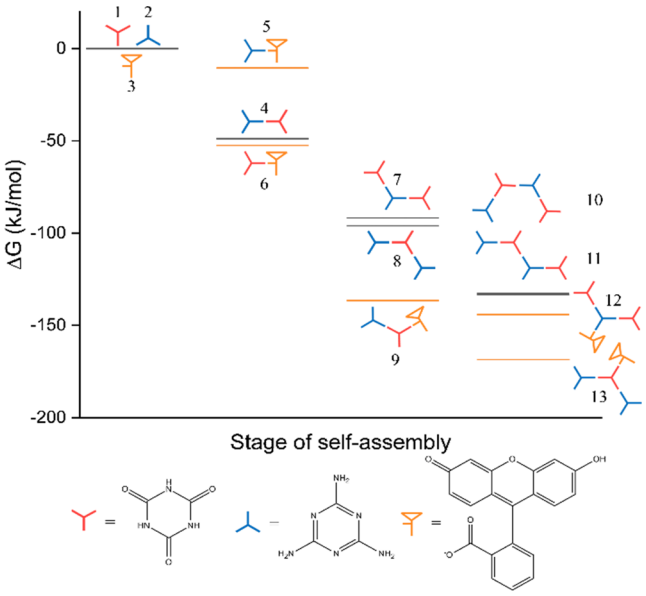

Figure 2. Formation energy comparison of M−CA with FITC molecular associations with respect to initial molecules. Gibbs free energies for formation of M−CA with FITC molecular associations.

does not follow the trend of decreasing energy observed in our previous work with melamine−barbituric acid complexes.[20] While the formation of a dimer (structure 4, Figure 2) from M and CA is an energetically profitable and probable process, the trimers (structures 7 and 8, Figure 2) have higher energies than the dimer. Both tetramers (structures 10 and 11, Figure 2) also have higher energies than trimers (it should be noted that the two possible forms of tetramers—arched and branched have roughly the same energies). Furthermore, the FL binding is a very energy-efficient process for all investigated complexes and individual cyanuric acid. It appears that the formation of the CA−FL dimer (structure 6, Figure 2) is more profitable than the formation of the M−CA dimer, while FL binding to the M (structure 5, Figure 2) is less energetically profitable. The M−CA−FL trimer (structure 9, Figure 2) is more thermodynamically stable than M−CA−M, CA−M−CA, and M−CA. FITC binds to trimers to form a more stable complex compared to the tetramers formed without fluorescein and individual trimers. It should be noted however that the M−CA−M−FL complex (structure 13, Figure 2) is preferred to the CA−M−CA−FL complex (structure 12, Figure 2).

Moreover, for the M−CA−M−FL complex (structure 13, Figure 2), the obtained optimized geometries feature protonation of the FL moiety by H^+ from CA. Therefore, it can be concluded that FL binding is probably happening in the first stages of self-assembly—it can either bind to individual cyanuric acid or to already existing M−CA dimer in the solution (since the energy gap between these two structures is considerably small), but the formation of the fluorescein monoanionic associates with larger M−CA complexes is energetically profitable in any case.

DFT analysis of a bigger associate than an adduct of the M−CA rosette bonded to FL is complicated by both the huge number of possible conformations and the exponential growth of the calculation duration. In this regard, it was decided to use the methods of molecular dynamics (MD), where these restrictions are partially removed.

Molecular Dynamics. Twenty independent molecular dynamics (MD) simulations were performed both in the presence and absence of FL to study the influence of FL on the kinetics of M−CA crystal nucleation in water solutions. Whereas DFT analysis gives information on the geometry and energetic stability of small molecular complexes, here, the analysis is expanded to include a larger scale and discuss how FL integrates into nanoscale M−CA clusters. Each simulation box contained 16 000 water molecules, 40 CA, and 40 M. Half of the simulation boxes additionally contained one FL molecule. Initially, all organic molecules were deposited at random positions and the unit cell was kept at T = 500 K and constant volume for 10 ns to dissolve any possible molecular aggregates before the main MD run. Afterward, NPT (isothermal−isobaric ensemble) simulations at T = 300 K and P = 1 atm were run for 300ns. Similar to the case of pure M-CA systems in water solutions, in the early stages of nucleation we observed formation of needle-like crystallites. FL molecules randomly integrated[19] into the crystallites in the plane of particular M-CA layers (Figure 3). Due to its more sophisticated geometry, the FL molecule slightly perturbs rosette-shaped patterns of the M−CA crystal lattice. Nevertheless, FL tends to integrate into the M−CA crystallite in all of the performed simulations. Apart from its ability to form hydrogen bonds with M and CA, this structure is additionally stabilized by $\pi-\pi$ stacking between the large aromatic FL plane and overlaying/underlaying M−CA layers.

The mean first-passage time (MFPT) method[21−25] was applied to evaluate the nucleation rate directly from MD simulations; Figure 3a shows the mean time required for the formation of a cluster containing n molecules. Both curves demonstrate a typical sigmoidal shape with a plateau after $n \approx 25$ (approximate size of the critical nuclei). However, in the presence of FL, faster formation of critical nuclei is observed. Component analysis shows that on average the FL molecule is

https://doi.org/10.1021/acsomega.1c01124
ACS Omega 2021, 6, 17267−17275

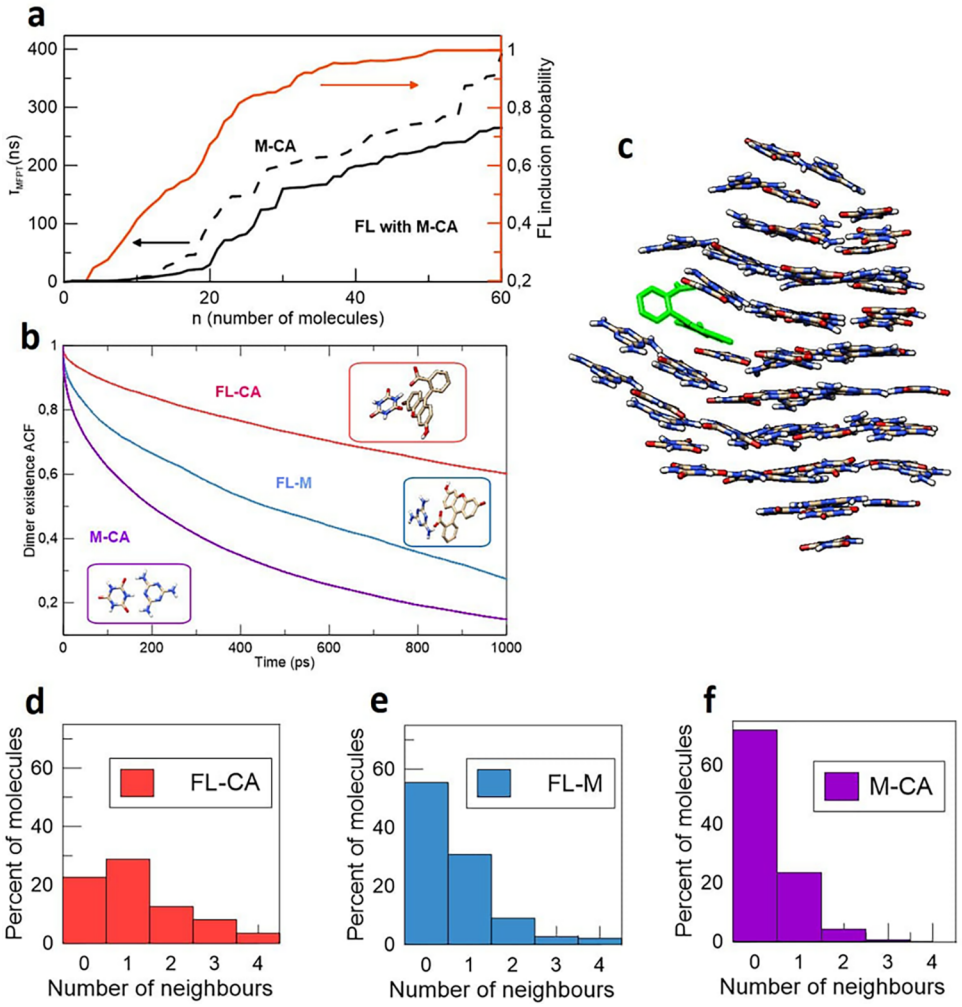

Figure 3. (a) Mean first-passage time (MFPT) curve for M−CA in water solutions with (solid line) and without (dashed line) FITC; (b) dimer existence autocorrelation functions for FITC−CA, FITC−M, and M−CA dimers; (c) M−CA nuclei with two FL molecules integrated into the crystal lattice (highlighted); (d−f) autocorrelation functions for FL−CA, FL−M, and M−CA dimers, respectively.

integrated into the cluster well before it reaches the critical size (red curve in Figure 3a). One can expect that at sufficient concentrations, FL molecules can play the role of initial seeds for nuclei formation. In agreement with DFT results (Figure 2), dimer existence autocorrelation analysis indicates that in water solutions FL forms more stable pair complexes with M and CA than M and CA form with each other (Figure 3c). Stability of FL−CA and FL−M dimers and the high mean number of neighboring molecules can also explain the enhanced nucleation rate observed for systems containing FL (Figure 3a).

UV−Vis Analysis of the Assembly and Disassembly of M−CA Capsules. Macroscale experimental observations of the self-assembly processes were studied by means of UV−vis spectroscopy. The intense fluorescence and pH sensitivity of sodium fluorescein make it an outstanding candidate for the experimental nondestructive observation of evolution of chemical reactions in reaction-diffusion systems. The changes in UV−vis spectra were used to monitor both assembly (Figure 4a) and disassembly of M−CA capsules in agarose gel, containing the fluorescent dye, under acidic (Figure 4b) and basic conditions (Figure 4c). Absorption spectra for both self-assembly and disassembly were similar to those obtained for the control experiments (Figure S3). In other words, neither melamine nor M−CA affects the inherent absorptivity of the various forms of sodium fluorescein molecules.[11] However, like the control experiments, melamine has a basic effect on the pH of the gel medium and subsequently favors the maximum absorbance of sodium fluorescein at 490 nm. This is countered by addition of cyanuric acid, which favors a hypsochromic shift toward 435 nm instead.

To compare the kinetic plots below, eq 1 was used to determine rate constants of the pseudo-first-order reactions of self-assembly and disassembly of the M−CA complex.

$$A_{+M} + CA \rightarrow k\ ^{A_{490\ nm}\downarrow}A_{+M\text{-}CA} \quad (1)$$

A_{+M} = absorbance at 490 nm in the presence of M (reactant).

CA = cyanuric acid.

$A_{+M\text{-}CA}$ = absorbance at 490 nm in the presence of melamine cyanurate (product).

k = rate constant for the pseudo-first-order reaction for absorbance at 490 nm.

$A_{490\ nm}\downarrow$ = decrease of absorbance at 490 nm.

A closer look reveals that maximum absorbance during capsule formation (ca 0.09 at 440 nm; time = 9 h) is relatively lower as time expires when compared to the control experiment (ca 0.16 at 435 nm; time = 9 h; Figure S3a). Two things could account for this occurrence. The first is that

https://doi.org/10.1021/acsomega.1c01124
ACS Omega 2021, 6, 17267−17275

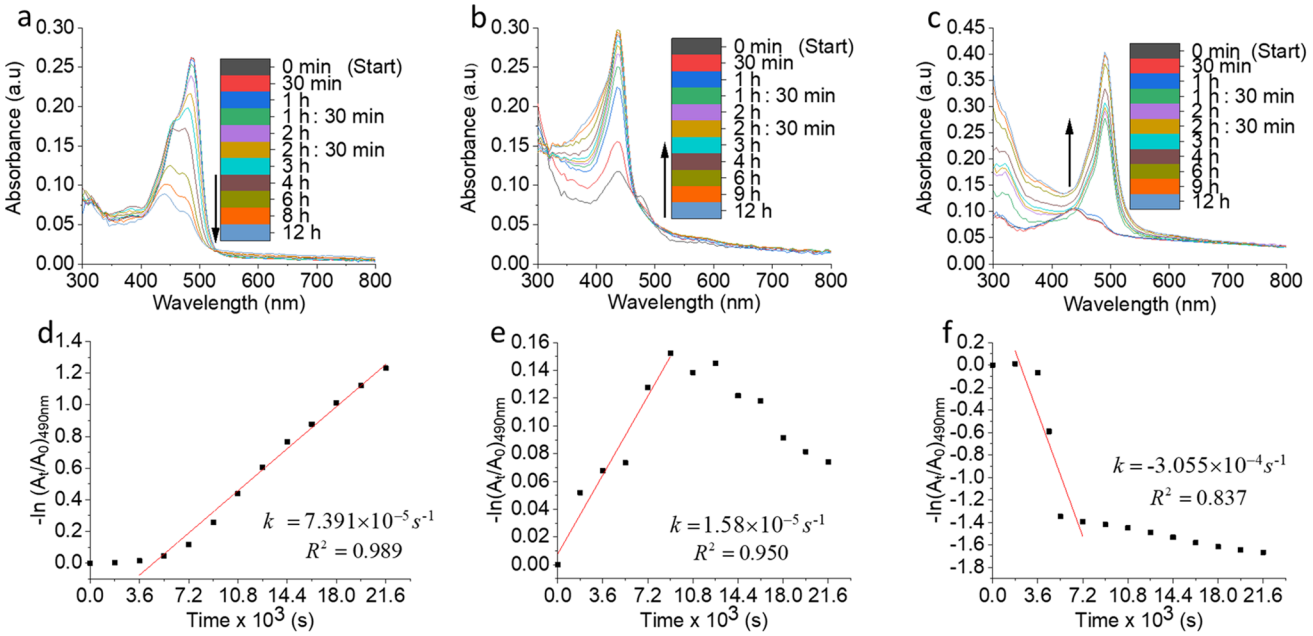

Figure 4. UV−vis absorption spectra taken periodically for (a) self-assembly of M−CA capsules, (b) disassembly of M−CA capsules at pH 4, and (c) disassembly of M−CA capsules at pH 9. Corresponding kinetic plots and pseudo-first-order linear fits placed underneath for (d) self-assembly of M−CA capsules, (e) disassembly of M−CA capsules at low pH levels, and (f) disassembly of M−CA capsules at high pH levels.

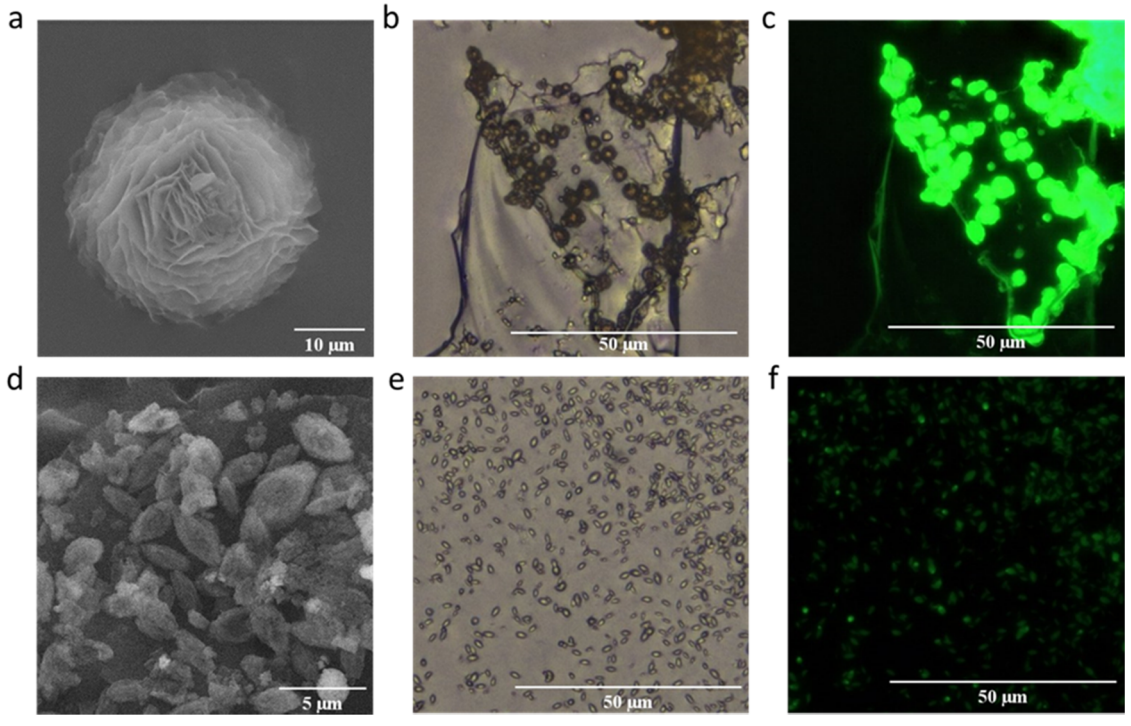

Figure 5. Scanning electron microscopy (a,d) and optical (b, c) and fluorescence (e, f) microscopy images of free (d−f) and occupied (a−c) M−CA structures.

M−CA traps FL molecules and therefore reduces the concentration of free fluorescent dye molecules. Since FL obeys Beer−Lambert's law, it implies that absorbance will decrease as more and more fluorescent dye molecules are trapped by M−CA capsules.[12] Also, as stated previously, the M−CA complex assembly is favored in a pH range that is mildly acidic[7,8] and such conditions are not ideal for the exclusive presence of the cationic form of FL that has the strongest absorptivity at 435 nm in a strongly acidic medium.[11,13]

The kinetic plot for self-assembly of M−CA capsules is linear after an hour, suggesting a uniform and gradual decline in the peak absorbance at 490 nm (Figure 4d). It also implies that there is a linear dependency of the presence of free sodium fluorescein molecules on the assembly of melamine cyanurate capsules. In other words, fluorescein is steadily used up as building material in the relatively slower process (k = 7.391 ×

https://doi.org/10.1021/acsomega.1c01124
ACS Omega 2021, 6, 17267−17275

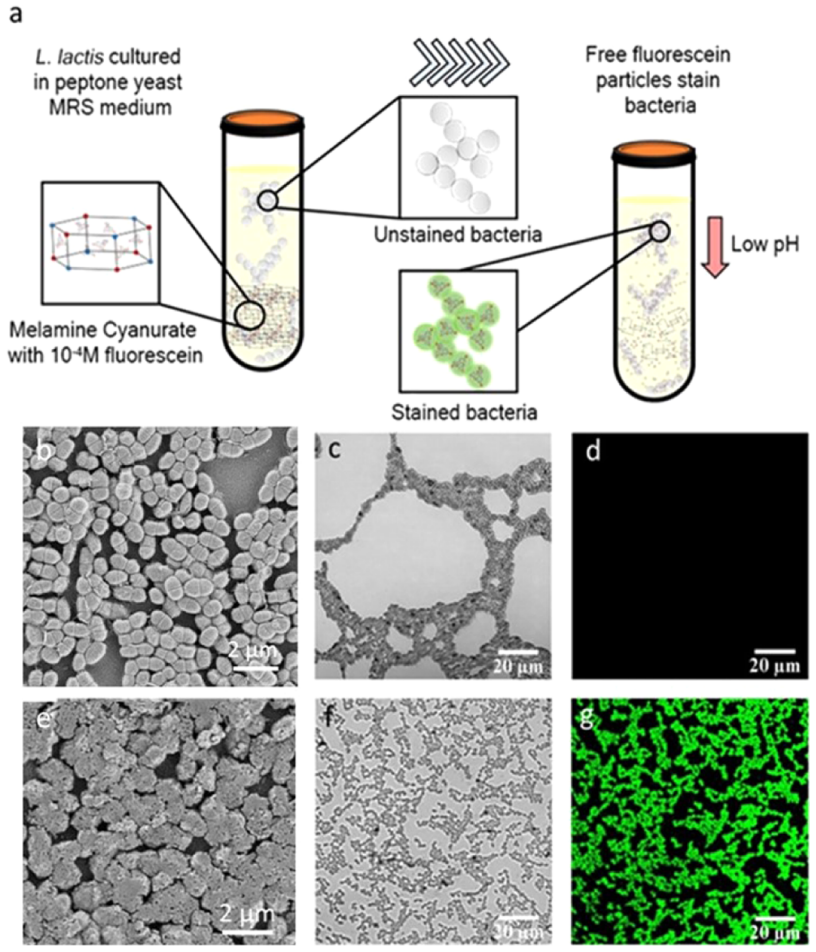

Figure 6. (a) Schematic illustrating the experiment involving the overnight culture of *L. lactis* 411 with sodium fluorescein encapsulated by melamine cyanurate capsules. Underneath the schematic are images of *L. lactis* 411 cultured overnight in the absence of encapsulated sodium fluorescein (b–d) and in the presence of encapsulated sodium fluorescein (e–g) using a scanning electron microscope (b and e) and fluorescence microscope (c, d, f, and g).

10^{-5} s^{-1}) of M–CA self-assembly. In comparison to the kinetic plot of the corresponding control experiment in Figure S3, self-assembly of capsules does slow the diffusion of cyanuric acid enough to affect its capacity to lower the pH. As previously stated, a low pH is required to decrease the absorbance at 490 nm and favor peak absorbance at 435 nm.[12]

The rate constant for the disassembly of melamine cyanurate capsules at low pH levels is the slowest (1.58×10^{-5} s^{-1}; Figure 4e), and unexpectedly, the kinetic plot that corresponds to this rate constant contrasts with that for the disassembly of melamine cyanurate capsules at high pH levels. Instead, it is similar to the kinetic plot for self-assembly of melamine cyanurate capsules because in an acidic medium it is expected that peak absorbance at 490 nm will decrease and peak absorbance at 435 nm will be favored, as observed in Figure 4b.[12] Also, it is likely that the presence of free melamine counters the pH effect of HCl appreciably, thus promoting a less acidic environment conducive for preserving M–CA capsules.

Disassembly of M–CA capsules at high pH levels on the other hand is about 4 times faster than the assembly of the capsules (Figure 4f). When compared to its corresponding control experiment (Figure S4), its rate constant is slightly lower with a difference of 0.687×10^{-4} s^{-1}. This suggests disassembly of capsules occurs quite rapidly and thus barely impedes the capacity of NaOH to diffuse through the agarose gel and increase the pH to 1 that favors peak absorbance at 490 nm. It is also worth stating that increasing absorbance values at 490 nm are also due (i) to increasing free FL molecules as M–CA capsules are disassembled and (ii) to some degree the presence of free M that promotes a neutral to basic medium.

An experiment on sequential assembly and disassembly of M–CA capsules was carried out to show the reversibility of the reaction. After the capsules were destroyed by the acid, the acid was neutralized by the addition of an equivalent amount of alkali, which led to the expected formation of a precipitate, which in turn was destroyed by the addition of an excess of alkali and again reduced by the acid to its original state. This shows, among other things, that the formation of capsules is not significantly influenced by inorganic ions.

Scanning Electron Microscopy (SEM) and Fluorescence Microscopy Images of Free and Occupied M–CA Capsules. M–CA capsules containing fluorescein (Figure 5a-c) were extracted from the agarose medium and compared to the fluorescein-free experiment (Figure 5d-f). Pure melamine cyanurate capsules form spindle-shaped aggregates. The capsules can be distinguished near the ends of the spindles, which could be associated with the oriented growth of initial needlelike crystals.[26] FL changes the shape significantly as well as enlarges the overall capsule size. The spherical shape

https://doi.org/10.1021/acsomega.1c01124
ACS Omega 2021, 6, 17267–17275

induced by the fluorescent dye could be attributed to inhibition of the nucleation stage and fast propagating radial growth from a single nucleus.[20] It should be noted that most nanostructures tend to form a sphere during fouling. Capsules containing FL do not exhibit anisotropic growth and form folded flat sheet spherical aggregates. Optical microscopy images also suggest that FL increases the size of capsules (Figure 5b) compared to pure M−CA (Figure 5e). Fluorescence microscopy shows a significant increase of luminescence intensity compared to M−CA (Figure S5), which indicates the presence of FL inside melamine cyanurate capsules (Figure 5c compared to Figure 5f). This is possibly due to incorporation of FL into melamine cyanurate capsules at the molecular level rather than incorporation of solution droplets containing sodium fluorescein as a distinct phase.

Low-pH Release of Encapsulated Fluorescent Dye Induced by *Lactococcus lactis*. Overnight cultures of *L. lactis* 411 were performed in peptone-yeast MRS medium. *L. lactis* significantly acidify the media with visible dissolution of formed M−CA precipitates. Afterward, the bacteria were centrifuged, washed several times, and placed on glass slides for study (Figure 6). Apart from acquiring a gritty surface texture against the much smoother appearance of bacteria in the control experiment, fluorescent bacteria fail to aggregate as observed for the control bacteria. There is no lysis of bacteria. The morphology of bacteria is different due to crystals (hexagonal ones) on their surface. The LIVE/DEAD BacLight Bacterial Viability Kit Protocol proves that bacteria are alive. We added schematics and further images (Figures S6−S9), where it is seen that there is another morphology of bacteria growing in the presence of FL due to crystal assembly on their surface rather than their lysis. Bacteria are alive; simultaneously, it is indeed, very interesting that they lost their tendency to agglomeration. This suggests that FL has an influence on bacterial aggregation and thus could have utility in controlling cellular behavior. A plausible explanation for these observations is that FL molecules surround the bacteria as they are encapsulating them, resulting in the coarse texture of stained bacteria. Also, the repulsion of like negative charges of FL shells could be responsible for its influence on the aggregation of bacteria. It is worth mentioning that FL being negatively charged should minimally interact with the negatively charged surface of bacteria, limiting staining of the cell surface or internalization. Here, the FL was chosen due to its ability to bind to functional biomolecules. While FL can bind to highly cationic species due to nonspecific electrostatic interactions, it has limited interactions with many biomolecules (especially negatively charged ones); otherwise, it would not be a particularly useful dye for use of the suggested capsules for tracking specific interactions in biology when conjugated to other probes.

CONCLUSIONS

Self-assembly of M−CA capsules occurs in both FL and non-FL media provided M and CA are present. However, fluorescent capsules are relatively larger and differ in shape when compared to empty capsules on a microscale. On a macroscale, the fluorescent capsules are visibly colored. Both DFT and molecular dynamics computations confirm the active participation of FL molecules in the early stages of the self-assembly process. Quantum chemical calculations show the energetic advantage of a process involving a fluorescein molecule. Active inclusion of FL into M−CA capsules is traced at the macroscopic level by observing time-dependent changes in visible spectra during capsule formation. Disassembly and subsequent release of trapped sodium fluorescein molecules occur under both low- and high-pH conditions with a markedly higher rate under high-pH conditions. The successful release of trapped fluorescein molecules by *L. lactis* acidification and observation of living bacteria prove biocompatibility of M−CA capsules and suggest a possible application of the M−CA assembly to be used as a prospective analyte for time-prolonged bacterial staining and retrospective monitoring of the pH shift below 4.8 in biological media.

EXPERIMENTAL SECTION

Chemicals. Agar (A7921; powder; CAS 9002-18-0), cyanuric acid 98% (1,3,5-triazine-2,4,6-triol; $(CNOH)_3$; 129.07 g mol^{-1}; Sigma-Aldrich, CAS 108-80-5), melamine (1,3,5-triazine-2,4,6-triamine; $C_3(HN)_6$; 126.12 g mol^{-1}; Sigma-Aldrich, CAS 108-78-1), sodium hydroxide (NaOH; 39.997 g mol^{-1}; Lenreaktiv, 130109 LR), hydrochloric acid (HCl; 36.46 g mol^{-1}; Lenreaktiv), sodium fluorescein ($C_{20}H_{10}Na_2O_5$; 376.27 g mol^{-1}), and peptone-yeast MRS medium were used. Distilled water from Millipore Elix (18 MΩ·cm^2/cm) was used to prepare the solutions for all experiments.

Quantum Chemical Computations. The full geometry optimization for all model structures was carried out at the B3LYP-D3/def2-SVP level of theory with the help of the Orca 4.2.1 program package.[26] The RIJCOSX approximation[27−29] utilizing the def2-SVP/C auxiliary basis set and spin-restricted approximation was employed. The convergence tolerances for the geometry optimization are as follows: energy change = 5.0 × 10^{-6} Eh, maximal gradient = 3.0 × 10^{-4} Eh/Bohr, RMS gradient = 1.0 × 10^{-4} Eh/Bohr, maximal displacement = 4.0 × 10^{-3} Bohr, and RMS displacement = 2.0 × 10^{-3} Bohr. The coupled perturbed self-consistent filed (CPSCF) equations were solved using the conjugate gradient (CG) method with convergence tolerance on a residual of 1.0 × 10^{-6} Eh. The Hessian matrices were calculated for all optimized model structures to prove the location of correct stationary points on the potential energy surfaces (no imaginary frequencies were found in all cases) and to estimate the thermodynamic properties (viz., enthalpy, entropy, and Gibbs free energy) for all model systems at 298.15 K and 1 atm. The Cartesian atomic coordinates for all optimized equilibrium model structures are available upon request.

Molecular Dynamics Simulation Details. MD simulations of melamine cyanurate aggregation in the presence of fluorescein were performed using the OpenMM package.[30,31] The method is discussed in detail by Orekhov et al.[6] Interatomic interactions were described by the all-atom optimized potentials for liquid simulations (OPLS-AA) force field[31,32] (which is known to reproduce hydration free energies of amino acids quite well[33]) with partial charges parameterized by LigParGen.[34−36] The TIP4P[37] rigid nonpolarizable model was used to parameterize the water molecules. A cutoff for short-range and nonbonded interactions was 1.2 nm. The smooth particle-mesh Ewald scheme[38] was used for long-range Coulomb interactions. Spatial distribution functions and DACFs were calculated using the TRAVIS software package.[39] Constant-temperature/constant-pressure simulations were performed at T = 300 K and P = 1 atm in the cubic unit cell with periodic boundary conditions containing 16 000 water molecules (approximate size 79 × 79 × 79 $Å^3$). The

https://doi.org/10.1021/acsomega.1c01124
ACS Omega 2021, 6, 17267−17275

integration timestep for all simulations was 2 fs. For cluster analysis, a cluster represented a group of molecules, each of which lies within r_{clust} = 7 Å cutoff with at least one other molecule. The visualization is done with the USCF Chimera package.[20]

UV−vis Analysis of the Assembly and Disassembly of Melamine Cyanurate Capsules. Three milliliters of dyed hot agarose gel, containing 1 mM melamine, was pipetted into cuvettes for all optical investigations using an Agilent Cary 60 UV−vis spectrophotometer. To run a time series UV−vis investigation for formation of capsules in the gel medium, 1 mL of 10 mM cyanuric acid was added to the gel medium and allowed to diffuse through the full length of the hydrogel, which causes the formation of M−CA capsules. Afterward, either 1 mL of 0.5 M HCl or 0.5 M NaOH was added to the gel medium to replace cyanuric acid as the diffusing solution to run a time series UV−vis investigation for dissolution of capsules at low or high pH levels, respectively. A control experiment without melamine keeping all other conditions the same was carried to investigate the role of M−CA capsules. Prior to all diffusion experiments, the calibration curve of the FL UV−vis absorption maximum position was prepared by measuring UV−vis spectra of 10^{-5} M FL in acetic (2.0−5.0), phosphate (6.0−8.0), and ammonia (9.0−12.0) buffer solutions. All of the solutions were verified with a laboratory pH meter calibrated with a series of standard buffer solutions (4.01/7.01/9.18).

Scanning Electron Microscopy and Fluorescence Microscopy Images of Free and Occupied Melamine Cyanurate Capsules. Scanning electron microscopy images were obtained for pure melamine cyanurate capsules and melamine cyanurate capsules containing fluorescent dye (10^{-4} M sodium fluorescein) at an operating voltage of 20 kV. Prior to microscopy, the samples were extracted by melting the agarose gel at 80 °C, diluting the suspension with hot water, and then centrifuging at 6000 rpm for 5 min in 2 mL Eppendorf tubes to obtain particles. The operation was repeated thrice to remove all excess gel. The particles that remained were mounted on carbon tape and covered with a thin platinum−gold alloy layer. Fluorescence imaging was carried out with a dry ×40 lens with a total magnification of ×400 on the image using the FITC channel (excitation 480 nm/emission 527 nm). Other imaging parameters like exposure, gain, aperture, and intensity were also kept constant throughout the experiment for comparison purposes. Before imaging, a 1 mm diameter thin-wall capillary tube was used to extract gel containing capsules. The capsules were placed on a slide and rinsed with distilled water. The setup was left undisturbed for at least 10 min before imaging. Microluminescence spectra and corresponding full visible spectrum luminescence images were acquired using a Zeiss Axio Imager.A2m equipped with an Ocean Optics QE Pro spectrometer (excitation by HAL 100 and HBO 100).

Low-pH Release of Encapsulated Fluorescent Dye Induced by *L. lactis* ssp. lactis 411 (*L. lactis*) Acidification. Overnight cultures were performed in peptone-yeast MRS medium with both a piece of pure agar gel containing free melamine cyanurate capsules and another piece of agar gel containing melamine cyanurate capsules with 10^{-4} M FL (see the schematics in Figure S6). After overnight culturing, the bacteria were centrifuged, washed several times, and placed on glass slides. Samples were dried and sputtered with the Au layer for the SEM study. The bacteria were also tested by the LIVE/DEAD BacLight Bacterial Viability Kits. This method provides a sensitive, fluorescence-based assay for bacterial cell viability. The reagent employs two nucleic acid stains: the green-fluorescent SYTO 9 stain and the red-fluorescent propidium iodide stain. Live bacteria with intact membranes fluoresce green, while dead bacteria with damaged membranes fluoresce red. All bacteria were alive. For bacterial imaging, we use both scanning electron microscopy (SEM) and fluorescence microscopy (FITC mode).

■ ASSOCIATED CONTENT

Supporting Information

The Supporting Information is available free of charge at https://pubs.acs.org/doi/10.1021/acsomega.1c01124.

Structures used for DFT calculations, images of M−CA structures formed in the presence of various concentrations of FL, further kinetics study, microluminescence spectra, and schematics and microscopy images of bacterial experiments (PDF)

■ AUTHOR INFORMATION

Corresponding Author

Ekaterina V. Skorb − *ITMO University, St. Petersburg 191002, Russian Federation;* orcid.org/0000-0003-0888-1693; Email: skorb@itmo.ru

Authors

Nfayem Imoro − *ITMO University, St. Petersburg 191002, Russian Federation*

Vladimir V. Shilovskikh − *ITMO University, St. Petersburg 191002, Russian Federation*

Pavel V. Nesterov − *ITMO University, St. Petersburg 191002, Russian Federation*

Alexandra A. Timralieva − *ITMO University, St. Petersburg 191002, Russian Federation*

Dmitry Gets − *ITMO University, St. Petersburg 191002, Russian Federation;* orcid.org/0000-0001-6288-2123

Anna Nebalueva − *ITMO University, St. Petersburg 191002, Russian Federation*

Filipp V. Lavrentev − *ITMO University, St. Petersburg 191002, Russian Federation*

Alexander S. Novikov − *ITMO University, St. Petersburg 191002, Russian Federation*

Nikolay D. Kondratyuk − *Moscow Institute of Physics and Technology, Moscow Region 141701, Russian Federation; Joint Institute for High Temperatures of the Russian Academy of Sciences, Moscow 125412, Russian Federation*

Nikita D. Orekhov − *Moscow Institute of Physics and Technology, Moscow Region 141701, Russian Federation; Joint Institute for High Temperatures of the Russian Academy of Sciences, Moscow 125412, Russian Federation; Bauman Moscow State Technical University, Moscow 105005, Russia*

Complete contact information is available at: https://pubs.acs.org/10.1021/acsomega.1c01124

Notes

The authors declare no competing financial interest.

■ ACKNOWLEDGMENTS

The work is supported by a grant from RFBR (No. 20-53-00043).

REFERENCES

(1) Skorb, E. V.; Möhwald, H. Dynamic Interfaces for Responsive Encapsulation Systems. *Adv. Mater.* **2013**, *25*, 5029−5043.
(2) Skorb, E. V.; Skirtach, A.; Sviridov, D. V.; Shchukin, D. G.; Möhwald, H. "Smart" Laser-Controllable Coatings for Corrosion Protection. *ACS Nano* **2009**, *3*, 1753−1760.
(3) Nikitina, A. A.; Ulasevich, S. A.; Kassirov, I. S.; Bryushkova, E. A.; Koshel, E. I.; Skorb, E. V. Nanostructured Layer-by-Layer Polyelectrolyte Containers to Switch Biofilm Fluorescence. *Bioconjugate Chem.* **2018**, *29*, 3793−3799.
(4) Gensel, J.; Borke, T.; Pérez, N. P.; Fery, A.; Andreeva, D. V.; Betthausen, E.; Müller, A. H. E.; Möhwald, H.; Skorb, E. V. Cavitation Engineered 3D Sponge Networks and Their Application in Active Surface Construction. *Adv. Mater.* **2012**, *24*, 985−989.
(5) Sedlmayer, F.; Jaeger, T.; Jenal, U.; Fussenegger, M. Quorum-Quenching Human Designer Cells for Closed-Loop Control of *Pseudomonas aeruginosa* Biofilms. *Nano Lett.* **2017**, *17*, 5043−5050.
(6) Orekhov, N.; Kondratyk, N.; Logunov, M.; Timralieva, A.; Shilovskikh, V.; Skorb, E. V. Insights into the Early Stages of Melamine Cyanurate Nucleation from Aqueous Solution. *Cryst. Growth Des.* **2021**, *21*, 1984−1992.
(7) Ma, M.; Bong, D. Determinants of Cyanuric Acid and Melamine Assembly in Water. *Langmuir* **2011**, *27*, 8841−8853.
(8) Jang, Y. H.; Hwang, S.; Chang, S. B.; Ku, J.; Chung, D. S. Acid Dissociation Constants of Melamine Derivatives from Density Functional Theory Calculations. *J. Phys. Chem. A* **2009**, *113*, 13036−13040.
(9) Kumar, M.; Ing, N. L.; Narang, V.; Wijerathne, N. K.; Hochbaum, A. I.; Ulijn, R. V. Amino-acid-encoded biocatalytic self-assembly enables the formation of transient conducting nanostructures. *Nat. Chem.* **2018**, *10*, 696−703.
(10) Smith, S. A.; Pretorius, W. A. Spectrophotometric determination of pKa values for fluorescein using activity coefficient corrections. *Water SA* **2002**, *28*, 395−402.
(11) Klonis, N.; Sawyer, W. H. Spectral properties of the prototropic forms of fluorescein in aqueous solution. *J. Fluoresc.* **1996**, *6*, 147−157.
(12) Doughty, M. J. pH dependent spectral properties of sodium fluorescein ophthalmic solutions revisited. *Ophthalmic Physiol. Opt.* **2010**, *30*, 167−174.
(13) Albright, V.; Zhuk, I.; Wang, Y.; Selin, V.; Belt-Gritter, B.; Busscher, H. J.; Mei, H. C.; Sukhishvili, S. A. Self-defensive antibiotic-loaded layer-by-layer coatings: Imaging of localized bacterial acidification and pH-triggering of antibiotic release. *Acta Biomater.* **2017**, *61*, 66−74.
(14) Malkappa, K.; Ray, S. S. Thermal Stability, Pyrolysis Behavior, and Fire-Retardant Performance of Melamine Cyanurate@Poly(cyclotriphosphazene-co-4,4′-sulfonyl diphenol) Hybrid Nanosheet-Containing Polyamide 6 Composites. *ACS Omega* **2019**, *4*, 9615−9628.
(15) Gijsman, P.; Steenbakkers, R.; Fürst, C.; Kersjes, J. Differences in the flame retardant mechanism of melamine cyanurate in polyamide 6 and polyamide 66. *Polym. Degrad. Stab.* **2002**, *78*, 219−224.
(16) Korolkov, V. V.; Timokhin, I. G.; Haubrichs, R.; Smith, E. F.; Yang, L.; Yang, S.; Champness, N. R.; Schröder, M.; Beton, P. H. Supramolecular networks stabilise and functionalise black phosphorus. *Nat. Commun.* **2017**, *8*, No. 1385.
(17) Roy, B.; Bairi, P.; Nandi, A. K. Supramolecular assembly of melamine and its derivatives: nanostructures to functional materials. *RSC Adv.* **2014**, *4*, 1708−1734.
(18) Staniec, P. A.; Perdigão, L. M. A.; Rogers, B. L.; Champness, N. R.; Beton, P. H. Honeycomb Networks and Chiral Superstructures Formed by Cyanuric Acid and Melamine on Au(111). *J. Phys. Chem. C* **2007**, *111*, 886−893.
(19) Song, A.; Zhang, J.; Zhang, M.; Shen, T.; Tang, J. Spectral properties and structure of fluorescein and its alkyl derivatives in micelles. *Colloids Surf., A* **2000**, *167*, 253−262.
(20) Skorb, E. V.; Shilovskikh, V. V.; Timralieva, A. A.; Nesterov, P. V.; Novikov, A. S.; Sitnikov, P. A.; Konstantinova, E. A.; Kokorin, A. I. Melamine−Barbiturate Supramolecular Assembly as a pH-Dependent Organic Radical Trap Material. *Chem. - Eur. J.* **2020**, *26*, 16603−16610.
(21) Pettersen, E. F.; Goddard, T. D.; Huang, C. C.; Couch, G. S.; Greenblatt, D. M.; Meng, E. C.; Ferrin, T. E. UCSF Chimera—A Visualization System for Exploratory Research and Analysis. *J. Comput. Chem.* **2004**, *25*, 1605−1612.
(22) Wedekind, J.; Strey, R.; Reguera, D. New method to analyze simulations of activated processes. *J. Chem. Phys.* **2007**, *126*, No. 134103.
(23) Chkonia, G.; Wölk, J.; Strey, R.; Wedekind, J.; Reguera, D. Evaluating nucleation rates in direct simulations. *J. Chem. Phys.* **2009**, *130*, No. 064505.
(24) Pisarev, V. V. Nonclassical nucleation kinetics in the crystallization of a supercooled melt. *Russ. J. Phys. Chem. A* **2014**, *88*, 1382−1387.
(25) Yuhara, D.; Barnes, B. C.; Suh, D.; Knott, B. C.; Beckham, G. T.; Yasuoka, K.; Wu, D. T.; Sum, A. K. Nucleation rate analysis of methane hydrate from molecular dynamics simulations. *Faraday Discuss.* **2015**, *179*, 463−474.
(26) Kharisov, B. I. *Handbook of Less-Common Nanostructures*; CRC Press: Boca Raton, FL, USA, 2012.
(27) Neese, F. The ORCA program system. *Wiley Interdiscip. Rev. Comput. Mol. Sci.* **2012**, *2*, 73−78.
(28) Neese, F.; Wennmohs, F.; Hansen, A.; Becker, U. Efficient, approximate and parallel Hartree−Fock and hybrid DFT calculations. A 'chain-of-spheres' algorithm for the Hartree−Fock exchange. *Chem. Phys.* **2009**, *356*, 98−109.
(29) Neese, F. An improvement of the resolution of the identity approximation for the formation of the Coulomb matrix. *J. Comput. Chem.* **2003**, *24*, 1740−1747.
(30) Eastman, P.; Swails, J.; Chodera, J. D.; McGibbon, R. T.; Zhao, Y.; Beauchamp, K. A.; Wang, L.-P.; Simmonett, A. C.; Harrigan, M. P.; Stern, C. D.; Wiewiora, R. P.; Brooks, B. R.; Pande, V. S. OpenMM 7: Rapid development of high performance algorithms for molecular dynamics. *PLoS Comput. Biol.* **2017**, *13*, No. e1005659.
(31) Friedrichs, M. S.; Eastman, P.; Vaidyanathan, V.; Houston, M.; Legrand, S.; Beberg, A. L.; Ensign, D. L.; Bruns, C. M.; Pande, V. S. Accelerating molecular dynamic simulation on graphics processing units. *J. Comput. Chem.* **2009**, *30*, 864−872.
(32) Jorgensen, W. L.; Maxwell, D. S.; Tirado-Rives, J. Development and Testing of the OPLS All-Atom Force Field on Conformational Energetics and Properties of Organic Liquids. *J. Am. Chem. Soc.* **1996**, *118*, 11225−11236.
(33) Shirts, M. R.; Pitera, J. W.; Swope, W. C.; Pande, V. S. Extremely precise free energy calculations of amino acid side chain analogs: Comparison of common molecular mechanics force fields for proteins. *J. Chem. Phys.* **2003**, *119*, 5740−5761.
(34) Jorgensen, W. L.; Tirado-Rives, J. Potential energy functions for atomic-level simulations of water and organic and biomolecular systems. *Proc. Natl. Acad. Sci. U.S.A.* **2005**, *102*, 6665−6670.
(35) Dodda, L. S.; Vilseck, J. Z.; Tirado-Rives, J.; Jorgensen, W. L. 1.14*CM1A-LBCC: Localized Bond-Charge Corrected CM1A Charges for Condensed-Phase Simulations. *J. Phys. Chem. B* **2017**, *121*, 3864−3870.
(36) Dodda, L. S.; De Vaca, I. C.; Tirado-Rives, J.; Jorgensen, W. L. LigParGen web server: an automatic OPLS-AA parameter generator for organic ligands. *Nucleic Acids Res.* **2017**, *45*, W331−W336.
(37) Jorgensen, W. L.; Chandrasekhar, J.; Madura, J. D.; Impey, R. W.; Klein, M. L. Comparison of simple potential functions for simulating liquid water. *J. Chem. Phys.* **1983**, *79*, 926−935.
(38) Essmann, U.; Perera, L.; Berkowitz, M. L.; Darden, T.; Lee, H.; Pedersen, L. G. A smooth particle mesh Ewald method. *J. Chem. Phys.* **1995**, *103*, 8577−8593.
(39) Brehm, M.; Kirchner, B. TRAVIS-A Free Analyzer and Visualizer for Monte Carlo and Molecular Dynamics Trajectories. *J. Chem. Inf. Model.* **2011**, *51*, 2007−2023.

https://doi.org/10.1021/acsomega.1c01124
ACS Omega 2021, 6, 17267−17275